

Core-Alkynylated Fluorescent Flippers: Altered Ultrafast Photophysics to Track Thick Membranes

Khurnia Krisna Puji Pamungkas⁺, Ina Fureraj⁺, Lea Assies⁺, Naomi Sakai, Vincent Mercier, Xiao-Xiao Chen, Eric Vauthey,* and Stefan Matile*

In memory of Richard G. Weiss

Abstract: Fluorescent flippers have been introduced as small-molecule probes to image membrane tension in living systems. This study describes the design, synthesis, spectroscopic and imaging properties of flippers that are elongated by one and two alkynes inserted between the push and the pull dithienothiophene domains. The resulting mechanophores combine characteristics of flippers, reporting on physical compression in the ground state, and molecular rotors, reporting on torsional motion in the excited state, to take their photophysics to new level of sophistication. Intensity ratios in broadened excitation bands from differently twisted conformers of core-alkynylated flippers thus report on mechanical compression. Lifetime boosts from ultrafast excited-state planarization and lifetime drops from competitive intersystem crossing into triplet states report on viscosity. In standard lipid bilayer membranes, core-alkynylated flippers are too long for one leaflet and tilt or extend into disordered interleaflet space, which preserves rotor-like torsional disorder and thus weak, blue-shifted fluorescence. Flipper-like planarization occurs only in highly ordered membranes of matching leaflet thickness, where they light up and selectively report on these thick membranes with red-shifted, sharpened excitation maxima, high intensity and long lifetime.

Introduction

Core alkynylation of fluorescent probes has been realized in many variations.^[1–8] Core alkynylation stands here for the insertion of one or several carbon–carbon triple bonds, alternating with single bonds, between two parts of a fluorophore (Figure 1). Many examples focus on identical fluorophores at both termini, from substituted phenyls^[2,3,5,9–21] and pyridines^[6,19] to BODIPYs^[22–24] and porphyrins.^[1,7,25–27] Combinations for asymmetric but not polarizing core-alkynylated fluorophores cover phenyls,^[28,29] nucleosides,^[30] BODIPYs^[30] or anthracenes.^[28] With asymmetric core-alkynylation, push–pull chromophores have attracted much attention, with donors and acceptors attached to each end of the mono- and oligoynes.^[4,6,18] Realized examples include substituted phenyls,^[4,6,8,18,31–35] thiophenes,^[31–33] coumarins,^[36] BODIPYs,^[37] phenothiazines,^[38] porphyrins,^[8] tetrathiafulvalenes^[31] and fluorenes^[31] as donors and substituted phenyls,^[6,18,35,36] rhodamines,^[37] merocyanines,^[37] porphyrins,^[8] 2,5-diphenyl-1,3,4-oxadiazoles,^[31,34] 1,1,4,4-tetracyanobuta-1,3-dienes,^[4] naphthalimides,^[38] aldehydes^[39] and pyridiniums^[32] as acceptors. Core alkynylation separates the two parts of the chromophores in space. This usually excludes contacts between the chromophore part that would hinder rotation within the alkynylated core (*r*, Figure 1). The presence of two perpendicular p orbitals per carbon in the alkynylated core further lowers rotational barriers. As a result, equilibration between twisted conformers is almost barrier-free in the ground state, with only a slight preference for the fully conjugated planar conformer. For this reason, core-alkynylated fluorescent probes have emerged as privileged molecular rotors. Molecular rotors work based on torsional motion off equilibrium in the excited state and report increasing viscosity or confinement with increasing fluorescence intensity and lifetime but usually without shifts of excitation maxima.^[40]

Core-alkynylated push–pull chromophores are of particular interest to introduce strong dipoles in planar but not in twisted conformers to increase red shifts upon planarization. In several examples, core alkynylation has provided access to unique spectroscopic properties, such as selective excitation of differently twisted conformers, environmentally sensitive excited-state planarization, and so on.^[1,27,35] Mechanical and chemical control over the torsional disorder of core-alkynylated systems has been used to visualize viscos-

[*] Dr. K. K. P. Pamungkas,⁺ Dr. L. Assies,⁺ Dr. N. Sakai, Dr. X.-X. Chen, Prof. S. Matile

Department of Organic Chemistry, University of Geneva, Geneva, Switzerland

E-mail: stefan.matile@unige.ch

Homepage: www.unige.ch/sciences/chiorg/matile/

Dr. I. Fureraj,⁺ Prof. E. Vauthey

Department of Physical Chemistry, University of Geneva, Geneva, Switzerland

E-mail: eric.vauthey@unige.ch

Dr. V. Mercier

ACCESS Geneva, University of Geneva, Geneva, Switzerland

[†] These three authors contributed equally to this study.

© 2024 The Authors. *Angewandte Chemie International Edition* published by Wiley-VCH GmbH. This is an open access article under the terms of the Creative Commons Attribution License, which permits use, distribution and reproduction in any medium, provided the original work is properly cited.

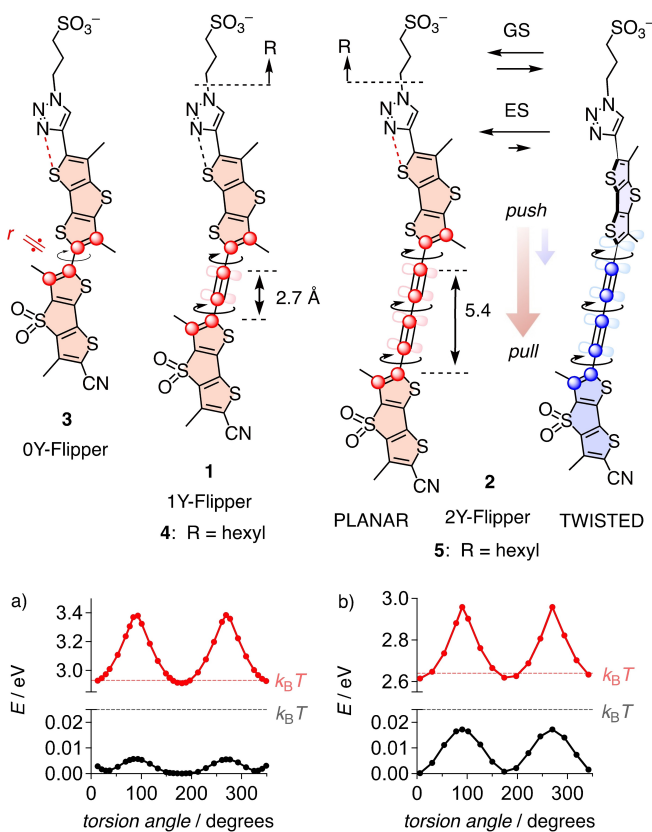


Figure 1. Core-alkynylated flippers **1** with one triple bond (1Y-Flipper) and **2** with two triple bonds (2Y-Flipper) compared to original non-alkynylated 0Y-Flipper **3**, with indication of pertinent p orbitals (lobes, circles), rotatable bonds (curved arrows), distances in Å (double headed arrows), repulsion (*r*), conformational equilibria in ground (GS) and excited state (ES) and push-pull dipoles (downward arrows). a, b) Energy of **4** (a) and **5** (b) in the S_0 (black, bottom) and S_1 states (red, top) as a function of the dihedral angle between the two dithienothiophene subunits. The horizontal dashed lines represent thermal energy at room temperature relative to the minimum energy in ground and excited state ($k_B T$).

ity, order,^[35] tension^[3,7,26,32] and potential^[8] in lipid bilayer membranes,^[1,8,32,33] polymersomes,^[7] polymer films,^[26] Langmuir–Blodgett (LB) monolayers^[2] and different interfaces, peptides^[35] for various sensing applications^[2,6,15] and artificial photosystems,^[2,6,14] and to elaborate on fundamental photophysical principles. Here we report core alkynylation of fluorescent flipper probes with one or two triple bonds, that is the synthesis and evaluation of 1Y-Flipper **1** and 2Y-Flipper **2** (Figure 1).

Fluorescent flippers like **3** without triple bonds in the core, i.e., 0Y-Flippers in the context of this study, have been introduced as small-molecule fluorescent probes for the imaging of membrane tension, i.e., a physical force, in living systems.^[41–43] These bioinspired^[44–46] planarizable push-pull probes^[46] are composed around an electron-rich and an electron-poor dithienothiophene. The two are twisted out of co-planarity by electrostatic repulsion around the rotatable central bond. Planarization in the ground state by physical compression establishes full conjugation. This turns on a

push-pull dipole that shifts the absorption to the red and increases fluorescence lifetime and intensity. The red-shifting responsiveness of flippers to physical compression in equilibrium in the ground state is opposite to molecular rotors, working off equilibrium in the excited state.

The red-shifting flipper planarization increases with the order of lipid bilayer membranes. It also increases with membrane tension because the response is dominated by reorganization, particularly the sorting out of stretchable lipids in highly ordered microdomains with most emissive planar flippers. Most recent progress with flipper probes includes the targeting of early endosomes,^[47,48] water-sensitive,^[49] photocleavable^[50] and chemically releasable^[51] probes, macrodipole removal,^[52] sulfoxime-bridged dithienothiophene acceptors,^[53] and the planarization on G-quartets.^[54]

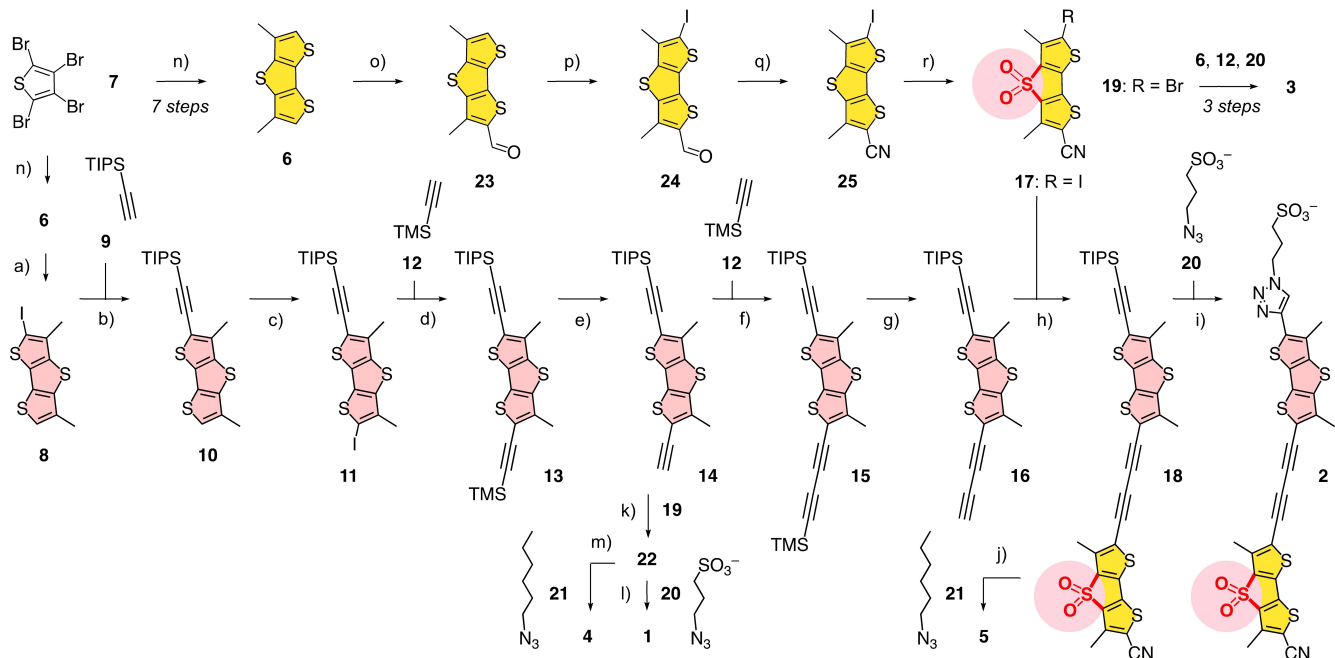
Small-molecule fluorescent probes,^[55,56,40,57–59] including flippers,^[41] that would target membranes depending on their thickness are nearly unexplored.^[3,45,60–63] The otherwise obvious strategy to use scaffolds of a length that matches the thickness of the membrane of interest is complicated by synthetic demand, solubility challenges and adaptive responses such as membrane swelling.^[60,64,65] More practical are α -helical scaffolds with easily variable length.^[64–68] They can be directly expressed in cells and labeled with bioengineered probes such as fluorescent proteins.^[66–68] These peptide-based approaches have so far not been engineered to image order and tension in membranes of a given thickness.

The here envisioned core alkynylation of 0Y-Flipper **3** elongates the rigid scaffold significantly, extends conjugation, removes repulsion in the core, and facilitates rotation in the core (Figure 1). In free solution, core-alkynylated 1Y-Flipper **1** and 2Y-Flipper **2** should thus exist with only a minor preference for planar conformers **p**, which is contrary to the strong preference of 0Y-Flipper **3** for twisted conformers **t** and provides access to unique photophysical properties. In membranes, the elongated rigid-rod scaffold^[45,61,69] of core-alkynylated **1** and **2** is most important to selectively image the order in thick, hydrophobically matching membranes.

Results and Discussion

Synthesis

The core-alkynylated 1Y-Flipper **1** and 2Y-Flipper **2** were synthesized together with the hydrophobic 1Y-analog **4** and 2Y-analog **5** from the unsubstituted dithienothiophene **6** (Scheme 1), which in turn was prepared from tetrabromo-thiophene **7** in 7 extensively optimized steps.^[41] Dithienothiophene **6** was mono-iodinated to give iododithienothiophene **8**, which was subjected to the Sonogashira coupling with TIPS-protected acetylene **9**. The resulting monoyne **10** was iodinated at the other terminus for another Sonogashira alkynylation of product **11**, this time with TMS-protected acetylene **12**. Removal of the more reactive TMS protecting group in **13** yielded the next key intermediate **14**, where the



Scheme 1. Synthesis of core-alkynylated flippers. a) NIS, $\text{CHCl}_3/\text{AcOH}$, 0°C to rt, 2 h, 82%; b) $\text{PdCl}_2(\text{PPh}_3)_2$, CuI , PPh_3 , $\text{THF}/\text{Et}_3\text{N}$, 80°C , 18 h, 76%; c) NIS, $\text{CHCl}_3/\text{AcOH}$, 0°C to rt, 2 h, 69%; d) $\text{PdCl}_2(\text{PPh}_3)_2$, CuI , PPh_3 , $\text{THF}/\text{Et}_3\text{N}$, 80°C , 18 h, 80%; e) K_2CO_3 , $\text{CH}_2\text{Cl}_2/\text{MeOH}$, rt, 2 h, 88%; f) $\text{NiCl}_2 \cdot 6\text{H}_2\text{O}$, CuI , TMEDA, THF , rt, 20 h, 37%; g) K_2CO_3 , $\text{CH}_2\text{Cl}_2/\text{MeOH}$, rt, 2 h, 66%; h) $\text{Pd}(\text{PPh}_3)_4$, $\text{THF}/\text{Et}_3\text{N}$, 60°C , 18 h, 88%; i) 1. TBAF, THF , rt, 1 h. 2. $\text{CuSO}_4 \cdot 5\text{H}_2\text{O}$, NaAsc, TBTA, $\text{CH}_2\text{Cl}_2/\text{H}_2\text{O}$, rt, 2 h. 3. TBACl, CH_3CN , rt, 5 min, 44% (TBA counterion); j) 1. TBAF, THF . 2. $\text{CuSO}_4 \cdot 5\text{H}_2\text{O}$, NaAsc, TBTA, $\text{CH}_2\text{Cl}_2/\text{H}_2\text{O}$, rt, 5 h, 23%; k) $\text{Pd}(\text{PPh}_3)_4$, $\text{THF}/\text{Et}_3\text{N}$, 80°C , 18 h, 76%; l) 1. TBAF, THF , $\text{CuSO}_4 \cdot 5\text{H}_2\text{O}$, NaAsc, TBTA, $\text{CH}_2\text{Cl}_2/\text{H}_2\text{O}$, rt, 3 h. 2. TBACl, CH_3CN , rt, 5 min, 40% (TBA counterion); m) TBAF, THF , $\text{CuSO}_4 \cdot 5\text{H}_2\text{O}$, NaAsc, TBTA, $\text{CH}_2\text{Cl}_2/\text{H}_2\text{O}$, rt, 24 h, 65%; n) 7 steps; o) POCl_3 , DMF , 90%;^[41] p) NIS, DMF , 80°C , 18 h, 86%; q) NaN_3 , TfOH , CH_3CN , 70°C , 1 h, 82%; r) *m*-CPBA, CHCl_3 , rt, 16 h, 26%.

syntheses of 1Y-Flipper **1** and 2Y-Flipper **2** diverged. For the slightly more demanding 2Y-Flipper **2**, another TMS-protected acetylene **12** was added using a Ni-catalyzed oxidative coupling.^[70] After selective cleavage of the TMS group in **15**, diyne **16** was coupled with the electron-deficient dithienothiophene **17**. The iodide leaving group was the key to successful generation of the desired product **18**, while the standard bromo analog **19** gave only a trace quantity of **18** and a major side product, temporarily assigned as homo coupled product of **16**, even under reducing conditions.^[71] With the 2Y-Flipper scaffold **18** in place, the TIPS group was cleaved and the sulfonate headgroup **20** clicked on to the terminal alkyne to afford the target amphiphile **2**. The hydrophobic 2Y-analog **5** was prepared by clicking alkyne **18** with n-alkyl azide **21**. 1Y-Flippers **1** and **4** were obtained analogously by coupling **14** with bromo-dithienothiophene oxide **19**, followed by TIPS removal, and clicking of the terminal alkyne in **22** with the azides **20** and **21**, respectively. Compound **17** was synthesized following the well-established protocol for **19** from dithienothiophene **6**^[41] by replacing the bromination step with iodination, i.e., iodination of **23**, installation of the nitrile acceptor from aldehyde **24**, and oxidation of the pseudo-sulfide bridge in **25**.

Overall, the synthesis of 1Y-Flipper **1** and 2Y-Flipper **2** and their hydrophobic analogs **4** and **5** was difficult but feasible. The main challenge was the poor solubility of the final push-pull compounds in most organic solvents. For amphiphiles **1** and **2**, counter-cation exchange with tetrabu-

tymmonium (TBA) was necessary to obtain solubilities high enough for NMR measurements. Equally challenging was the chromatographic purification of most intermediates because of their high hydrophobicity. This was particularly problematic with reactions that intrinsically produced product mixtures of nearly identical hydrophobicity. Yet, all intermediates were vigorously purified to ensure the high purity of final products.

Spectroscopic Properties in Solution

Quantum-chemical calculations on **4** and **5** predict planar minimum geometry in both the ground and the first singlet excited states (Figures 1a,b). However, rotation around the central bonds is free in the ground state at room temperature, whereas it is associated with a significant barrier in the S_1 state, namely 0.47 and 0.32 eV for **4** and **5**.

Consequently, the $S_1 \leftarrow S_0$ gap depends on the torsional angle with the minimum corresponding to the planar geometry. Therefore, excitation at the red-edge of the $S_1 \leftarrow S_0$ absorption band should preferentially photo-select planar molecules, whereas excitation at shorter wavelengths should interact with torsionally disordered flippers. This inhomogeneous broadening of the $S_1 \leftarrow S_0$ absorption band is supported by the spectral narrowing observed upon decreasing temperature (Figures 2a,b).

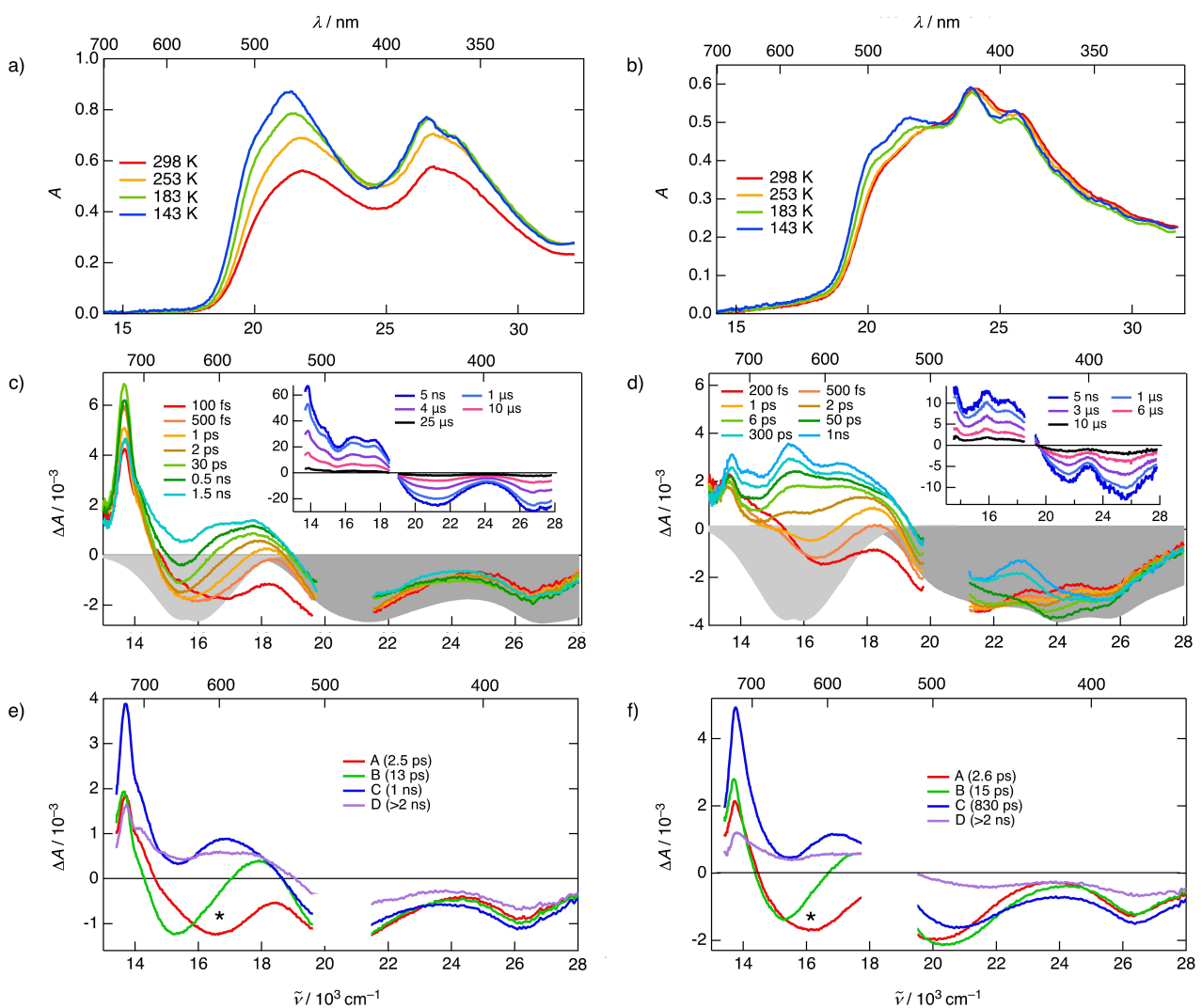


Figure 2. a, b) Stationary absorption spectrum of **4** (a) and **5** (b) in liquid methyl-tetrahydrofuran (MTHF) as a function of temperature. The weaker dependence measured with **5** relatively to **4** suggests a smaller torsional barrier for **5**. c, d) Early excited-state dynamics of **4** (c) and **5** (d) in CH_2Cl_2 recorded by transient absorption upon 483 nm excitation. Inset: late dynamics recorded after 532 nm excitation in CH_2Cl_2 purged with Ar. The negative stationary stimulated emission and absorption spectra are shown in grey. e, f) Evolution-associated difference absorption spectra and time constants obtained from a global analysis of the ultrafast transient absorption data recorded with **4** in benzonitrile upon band-maximum excitation (e) and red-edge (f) assuming a series of successive exponential steps ($\text{A} \rightarrow \text{B} \rightarrow \text{C} \rightarrow \text{D} \rightarrow$). * Note the larger red shift of the stimulated emission upon band-maximum excitation (e).

Transient absorption (TA) measurements with **4** were carried out in CH_2Cl_2 and benzonitrile upon excitation at the red edge (532 nm) and the maximum (483 nm) of the $\text{S}_1 \leftarrow \text{S}_0$ band (Figures 2c,e,f, S3–S6). The early TA spectra are dominated by negative bands due to the stimulated emission (SE) and the ground-state bleach (GSB), as well as by a positive band above 700 nm attributed to a $\text{S}_{n>1} \leftarrow \text{S}_1$ excited-state absorption. The SE band measured upon red-edge excitation is located at longer wavelength (617 nm, Figure 2f*) than upon band-maximum excitation (586 nm in CH_2Cl_2 , Figure 2c, red; 603 nm in benzonitrile, Figure 2e*). This can be attributed to the photo-selection of molecules with different degrees of torsion (Figure 1a). During the first 10–15 ps, the SE band red shifts to a location that is independent of the excitation wavelength (630 nm, Figure

es 2c,e,f). Upon band-maximum excitation, the SE intensity undergoes a small initial increase before decreasing like upon red-edge excitation (Figure 2c, orange). This effect can be assigned to the increase of oscillator strength for emission upon planarization (Figure S2), whereas the red shift can be attributed to both planarization and relaxation of the polar solvent around the excited state. These spectral changes were found to be faster in CH_2Cl_2 (Figures 2c, S4) than in benzonitrile (Figures 2e, S5), in agreement with the higher viscosity and slower relaxation dynamics of benzonitrile.^[72]

Once these processes are over, i.e., after a few tens of ps, the TA spectra remain essentially unchanged and decay on the ns timescale. These spectra can be assigned to the equilibrated planar S_1 state. Ns- μ s TA measurements upon 532 nm excitation reveal the occurrence of intersystem

crossing (ISC) to the T_1 state on the 1–2 ns timescale (Figure 2c, inset), in agreement with the 1.3 ns fluorescence lifetime of **4** (Figure S9). In turn, this state decays on a timescale ranging from hundreds of ns to tens of μ s (Figure 2c, inset), depending on the oxygen concentration (Figure S6). A triplet yield of the order of 50 % can be estimated from the intensity of the GSB.

Ultrafast TA measurements with **5** in CH_2Cl_2 upon 483 nm excitation point to similar initial dynamics dominated by planarization and solvent relaxation (Figures 2d, S7). Contrary to **4**, the SE band vanishes completely in a few tens of ps and the resulting TA spectrum remains almost unchanged up to the longest time delay of the experiment. According to ns- μ s TA measurements (Figure 2d, inset), this spectrum can be attributed to a triplet state as its decay accelerates from a few μ s to hundreds of ns in the presence of oxygen (Figure S8). A triplet yield close to unity can be estimated from the intensity of the GSB. This much faster ISC dynamics of **5** compared to **4** is confirmed by time-correlated single photon counting (TCSPC) measurements, which point to a non-exponential fluorescence decay with 95 % of the amplitude associated with a time constant close to the ~200 ps response function of the instrument (Figure S10).

Global analysis of the TA data assuming a series of successive exponential steps (A- $>$ B- $>$...) suggests that ISC in **5** cannot be associated with a single time constant (Figure S7). This is consistent with torsional disorder in the S_1 state directly after excitation and with ISC being faster for twisted than planar molecules. Perpendicular orientation of the two dithienothiophene sub-units should allow for much larger spin-orbit coupling than planar geometry and should, thus, considerably accelerate ISC.^[73–77] Because of the presence of two triple bonds in **5**, the torsional barrier in the S_1 state is lower than for **4** and, consequently, planarization is slower, leading to more efficient ISC (Figures 1a, b).

The impact of core alkynylation on rotational dynamics was further investigated by measuring the fluorescence viscosity dependence of alkyne Flippers **1**, **2**, and **3** in a mixture of EtOAc ($\eta=0.45$ cP) and triacetin ($\eta=23$ cP) at 20 °C (Figure 3). Poor solubility of probes did not allow measurements in more viscous solvents, such as castor oil, that would be desirable for comparison with lipid bilayer membranes.^[78,79]

All three compounds showed a viscosity-dependent enhancement of the lower energy excitation band, resulting in comparably small red shifts (Figure 3a–c). These changes were consistent with the increasingly hindered access from the twisted Franck–Condon state to the emissive planar intramolecular charge transfer (PICT) excited state in the more viscous media. The viscosity dependence of fluorescence intensity varied from flipper to flipper (Figure 3d). The 2Y-Flipper **2** showed typical behavior of molecular rotors with power-dependent fluorescence enhancement, consistent with the Förster-Hoffmann^[80] equation, and hindrance of the nonradiative rotational relaxation of the emissive excited state in the more viscous media (Figure 3d, ●). Similar fluorescence enhancement was

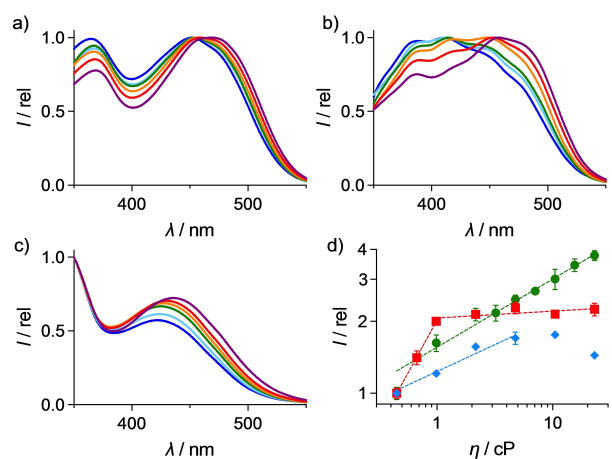


Figure 3. (a–c) Normalized excitation spectra of **1** (a), **2** (b), and **3** (c), all at 0.1 μM as TBA salts) in mixtures of EtOAc/triacetin (1:0 to 0:1, blue to dark red). (d) Integrated fluorescence intensities of **1** (■), **2** (●), and **3** (◆; $\lambda_{\text{ex}}=350$ –600 nm, $\lambda_{\text{em}}=650$ nm; mean \pm SEM) relative to those in EtOAc (=1) as a function of the viscosity of the solvents. Dashed lines represent the best fit to the Förster-Hoffmann equation.

observed with 0Y-Flipper **3** up to viscosity ≈ 10 cP and was followed by a diminution in more viscous solvents (Figure 3d, ◆). The latter behavior was as observed earlier in even more viscous media,^[61] and attributed to the decelerated planarization in the excited state. The fluorescence intensity of 1Y-Flipper **1** was nearly viscosity-independent, except for very low viscosity (Figure 3d, ■). Since the viscosity dependence of the excited state dynamics was evident from the TA studies (Figure 2c,e) and red-shifting excitation spectra (Figure 3a), the apparent viscosity independence of the intensity was attributed to the combination of the two effects, hindrance of planarization and rotational relaxation, which weaken and enhance fluorescence, respectively. The response to viscosity was overall minor compared to changes in matching membranes (see below), suggesting that like the original **3**, core expanded flippers **1** and **2** act in membranes more like flippers than like rotors, reporting on physical compression in the ground state rather than viscosity changes in the excited state.

Spectroscopic Properties in Lipid Bilayer Membranes

Original 0Y-Flippers like **3** report increasing order of lipid bilayer membranes with a large red shift of the excitation maximum and a strong increase in fluorescence intensity and lifetime, while the emission from the planar excited state does not change much.^[41] This signature responsiveness can be seen, for instance, in dipalmitoyl phosphatidylcholine large unilamellar vesicles (DPPC LUVs) upon transition from liquid-disordered (L_d , aka L_a) to solid-ordered (S_o , aka L_β) membranes at around 41 °C (Figure 4c). It is consistent with the physical compression of the favored twisted conformer of **3** to the disfavored planar conformer of **3** in the ground state (Figure 4b).

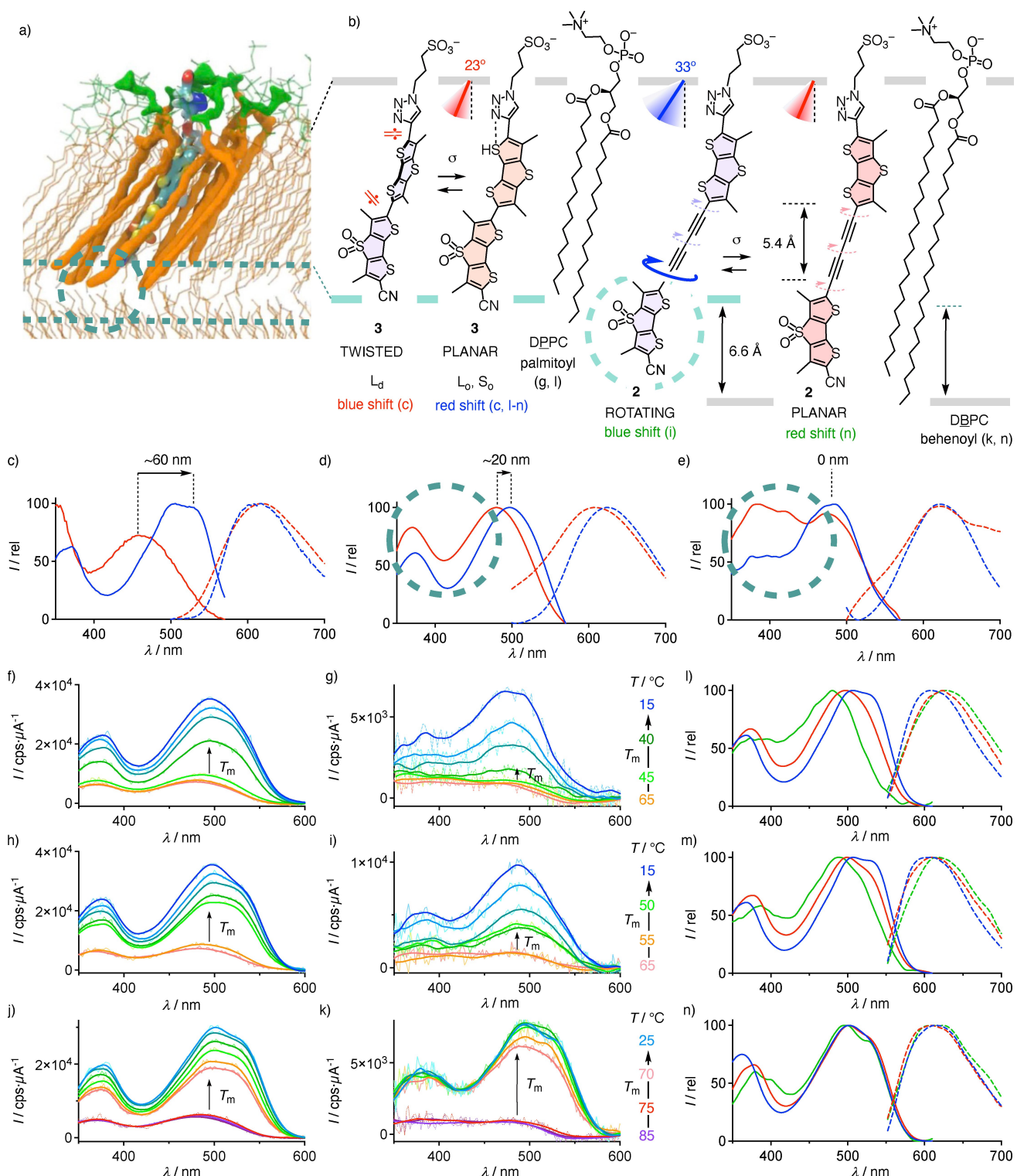


Figure 4. Core-alkynylated flippers track thick membranes. a) Computational model for the original flippers like **3** in solid-ordered membranes of matching thickness (DPPC), with indication of disordered interleaflet space accessible with elongated diynes **2** > monoynes **1** (dashed, green), adapted with permission from Ref. [81], © Royal Society of Chemistry, 2020. b) In standard ordered membranes (DPPC), matching **3** are planarized by physical compression at low tilting disorder (23°, SM/CL 7:3, see below), while the longer **2** stays oriented at higher tilting disorder (33°, SM/CL 7:3) and keeps rotating between the two leaflets (blue curved arrow). In thick ordered membranes (DBPC > DSPC), the elongated **2** > **1** match as well, stop rotating, planarize and emit selectively. c–e) Normalized excitation (solid) and emission spectra (dashed) of c) **3**, d) **1** and e) **2** (all at 25 nM) in DPPC LUVs at 65 (red) and 25 °C (blue), with the indication of red shift in excitation peaks with increasing order and absorption of twisted conformers (circles). f–k) Original (pale) and smoothed (dark) excitation spectra of **1** (f, h, j) and **2** (g, i, k; both at 3 nM) in DPPC (f, g), DSPC (h, i), or DBPC LUVs (j, k) upon cooling. l–n) Normalized smoothed excitation (solid) and emission (dashed) spectra of **2** (green), **1** (red) and **3** (blue) at 25 °C in DPPC (l), DSPC (m) and DBPC LUVs (n).

Core alkynylation in 1Y-Flipper **1** and 2Y-Flipper **2** reduced fluorescence intensity due to rotational quenching and ISC as described above. For monoyne **1** in DPPC LUVs (P=palmitoyl, C16:0), the ~60 nm red shift from L_d to S_o of original **3** decreased to ~20 nm (Figure 4d). For diyne **2**, the red shift from L_d to S_o DPPC LUVs was barely visible (Figure 4e). Instead, in L_d DPPC LUVs, the excitation maxima broadened strongly on the hypsochromic side and the spectrum became similar to the absorption spectrum of diyne **5** in solution (Figure 4e, green circle). In S_o DPPC LUVs, these hypsochromic bands were much weaker. Above ultrafast photophysics results implied that they originate from the excitation of twisted conformers of **2** (Figures 2e,f). Decreasing hypsochromic broadening with membrane order was thus consistent with decreasing accessibility of twisted 2Y-Flipper **2** to the emissive PICT state, as found in viscous solvents (Figure 4e, green circle). Interestingly, the relative intensity of the hypsochromic band was higher in L_d DPPC LUVs than in triacetin despite the higher reported viscosity of the former (≈ 50 cP),^[78] implying that more than just the viscosity is at play (Figures 4e,b). Less intense and as in solution (Figures 2,a), the same hypsochromic effect was also visible with 1Y-Flipper **1** (Figure 4d, green circle).

While sensitivity to membrane order was evidenced for 2Y-Flipper **2**, missing red shifts to the bathochromic maxima despite large Stokes shifts, missing vibronic structure and weak fluorescence intensity all implied that the ground-state planarization of 2Y-Flipper **2** in S_o DPPC LUVs is incomplete (Figure 4e). In contrast to 0Y-Flipper **3**, this incomplete planarization might suggest that the rigid-rod scaffold^[45,61,69] of 2Y-Flipper **2** is too long for one S_o DPPC leaflet and pushes one dithienothiophene into the less ordered interleaflet space, where rotor-like torsional motion is less restricted (Figure 4b). Molecular models of original 0Y-Flippers in DPPC membranes^[81] were consistent with this hypothesis (Figure 4a). The models showed nearly perfect matching lengths of the two, and the disordered interleaflet space opening up just below to accommodate the rotating dithienothiophene of 2Y-Flipper **2** (Figures 4a,b, green dashed lines, blue arrow).

This hypothesis was supported by the dependence of fluorescence intensity of diyne **2** in DPPC LUVs on temperature. The main transition T_m from fluid L_a into rippled P_b phase between 45 and 40°C passed almost unnoticed, and a gradual increase through gel L_b to respectable emission from the subgel L_c followed (Figure 4g). In contrast, the non-alkynylated flipper **3** reported T_m with a sharp increase followed by minor increases between P_b , L_b and L_c (Figure S21), and the intermediate monoyne **1** showed the intermediate behavior (Figure 4f). Such sharp changes were absent with 0-2Y Flippers **1-3** in DOPC LUVs (O=oleoyl, C18:1), which remain in L_d phase above -17°C (Figure S24). Temperature-dependent gradual increase in fluorescence intensity in the gel phase was as found previously with poorly positioned BODIPY rotors.^[82] Thus, the temperature-dependent changes of intensity and excitation maxima of alkyne flippers, **2** in particular, in DPPC LUVs were more rotor-like, consistent with our hypothesis

that a part of the probe locates in the interleaflet space of these too thin membranes.

Increasing leaflet thickness in DSPC LUVs (S=stearoyl, C18:0) gave preserved trends with an emerging T_m detectability between 55 and 50°C for diyne **2**, and almost exclusive T_m sensitivity for monoyne **1** (Figures 4h,i). These differences suggested that the length of monoyne **1** matches the thickness of DSPC leaflets, while diyne **2** is still too long and rotates in the disordered interleaflet space (Figures 4a,b).

In ultra-thick DBPC LUVs (B=behenoyl, C22:0), the sensitivity of the ultra-long 2Y-Flipper **2** for the T_m between 70°C and 75°C exceeded that of the shorter monoyne **1** (Figures 4j,k). Moreover, unlike in DPPC and DSPC, the excitation band of diyne **2** in L_b DBPC LUVs showed the distinct vibronic structure known from the non-alkynylated flipper **3** in L_b DPPC LUVs (Figure 4k vs c). These significant differences to the thinner DSPC (i) and DPPC (g) membranes suggested that hydrophobic matching in ultra-thick DBPC membranes affords rotation-free, planar 2Y-Flipper **2** exclusively (Figure 4b).

The conclusions from changes in fluorescence intensity were fully supported by changes in excitation maxima at 25°C. In DPPC, the excitation maxima blue shifted with flipper length, that is, increasing hydrophobic mismatch from the non-alkynylated **3** to monoyne **1** and diyne **2** (Figure 4l). Consistent with increasing hydrophobic matching, the excitation maxima in the thicker DSPC showed the same dependence on flipper length, but the differences between the maxima were smaller (Figure 4m). In the thickest DBPC, all excitation maxima overlapped at maximal red shift (Figure 4n). In comparison, emission spectra were less informative (Figures 4l-n, dashed lines). Still, the overall red shifts of emission maxima appear to coincide with blue shifts of excitation maxima, consistent with the poor localization in the membrane of hydrophobically mismatched flippers.

These consistent trends confirmed that for 2Y-Flipper **2**, rotation-free ground-state planarization occurs selectively in hydrophobically matching thick membranes. This differed from 0Y-Flipper **3**, which was planarized in ordered membranes independent of their thickness down to at least DPPC,^[83] and 1Y-Flipper **1** showing intermediate behavior. The doubly core-alkynylated 2Y-Flipper **2** thus selectively reported on unusually thick membranes of high order with red-shifted, sharpened and vibronically structured excitation maxima of higher intensity (Figure 4k, n vs l, green). Dominated by red-shifted excitation maxima, this selectivity of the extra-long **2** for hydrophobically matching thick membranes originated from flipper-like rather than rotor-like behavior, that is planarization of the twisted fraction of **2** (Figure 1) in equilibrium in the ground state by physical compression from the matching environment. Despite their high propensity to undergo ISC, alkyne flippers **1** and **2** were as photostable as **3** in L_d DOPC LUVs (Figure S26).

FLIM Properties in Lipid Bilayer Membranes

Fluorescence lifetime imaging microscopy (FLIM) of giant unilamellar vesicles (GUVs) composed of liquid-ordered (L_o) egg sphingomyelin/cholesterol (SM/CL) 7:3 afforded rapidly decreasing intensity and lifetimes with core alkynylation (Figure 5). This trend was consistent with increasing flipper deplanarization and torsional motion with increasing hydrophobic mismatch. The fluorescence decay profiles were complex, requiring 2–3 exponential fits (Figure S28), and thus analyzed using a phasor approach.^[84] This fit-free technique allows visualization of lifetime data by mathematically transforming the fluorescence decay of each pixel into points in a phasor plot (Figure 5, top). By selecting the cluster of phasor points, associated pixels can be identified in the mapped images (Figure 5, bottom). With flipper probes in GUVs, phasor clouds were found within the semicircles centered at $\tau \approx 4$ ns for 0Y-Flipper **3**, $\tau \approx 3$ ns for 1Y-Flipper **1** and $\tau \approx 2.5$ ns for 2Y-Flipper **2**, consistent with multiexponential decay.

The fluorescence lifetime of 1Y-Flipper **1** was not uniform. Both the fast FLIM image and the phasor analysis showed shorter lifetime near the poles compared to the equator regions (Figure 5b). FLIM images of all flippers in L_o membranes showed weaker fluorescence at the pole regions. These results were consistent with the excitation photoselection of oriented flippers in the membrane by the polarized laser. In contrast, FLIM images of 0Y-Flipper **3** in L_d membranes did not exhibit such intensity variations.^[41] These differences implied that **1** and **2** in L_o membranes are not tumbling like **3** in L_d membranes, but remain aligned along the ordered lipid tails. Then, the shortened fluorescence lifetime of **1** and **2** can be attributed to the increased torsional disorder in flippers that less perfectly align along the mismatched lipid tails and extend significantly beyond the leaflet into the less confining interleaflet space (Figure 4b).

Following the protocol of Gruszecki,^[85] the average angles (ν) between the transition dipoles of probes and the membrane axis normal were estimated from the intensity

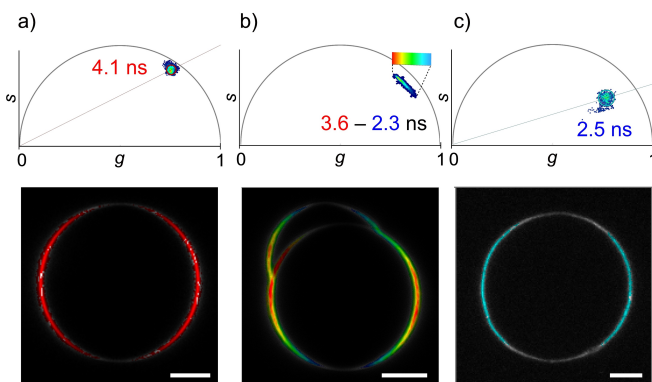


Figure 5. Phasor plots from fast FLIM images (top) and the color mapped intensity images of GUVs showing the origin of phasor spots (bottom) for 0Y-Flipper **3** (a), 1Y-Flipper **1** (b) and 2Y-Flipper **2** (c) in L_o membranes of SM/CL (7:3) GUVs; scale bars = 5 μ m.

ratios at the pole and the equator. The angles obtained might indicate average tilt angles if the probe orientation is uniform, which is unlikely to be the case with flippers, judging from the multiexponential decay profiles. Thus, we interpret these angles to indicate an average deviation from uniform flipper orientation, that is, positional disorder. Although the calculated $\nu = 23 \pm 2^\circ$ for original **3** would correlate reasonably well with the cholesterol tilt (0 – 18°) in L_o membranes,^[86–88] this small angle is thus best interpreted as a small deviation of probe alignment from parallel uniformity, that is low positional disorder (Figure 4b).

The larger $\nu = 33 \pm 3^\circ$ for **2** showed average positions adapted upon hydrophobic mismatch, extending from one leaflet into the less ordered intermembrane space with increasing deviation from uniform flipper alignment due to poorer complementarity with the confining environment (Figures 5c,b). Both extension into intermembrane disorder and growing positional disorder will increase rotor-like torsional motion in the excited state and thus produce the short lifetimes observed in the phasor plot.

The intermediate $\nu = 26 \pm 4^\circ$ for 1Y-Flipper **1** with intermediate mismatch revealed that the unique lifetime inhomogeneity in the phasor plot does not originate from increased deviation from uniform probe alignment (Figure 5b). Instead, this lifetime inhomogeneity could originate from populations of **1** in equally imperfect positions of matched **3** and mismatched **2** with long and short lifetimes, respectively.

Overall, these results from FLIM images of probes in L_o GUVs were in agreement with the results from S_o LUVs. Fluorescent lifetimes decreased with flipper elongation because of increasing torsional motion in oriented flippers, which stick out into the interleaflet space where they continue to rotate and thus shorten fluorescence lifetime by rotor-like torsional motion in the excited state. The observed increase in positional disorder of elongated flippers in L_o mismatched membranes was small compared to that of flippers in L_d membranes independent of their length, leading to the known completely homogeneous emission from GUVs in FLIM images. Thus, not only in S_o but also in L_o membranes, the length of the probe relative to the thickness of a leaflet is a critical factor for its positioning and function in membranes.

Consistent with experience and literature, attempts to produce DBPC GUVs with extra-thick membranes were not successful.

Conclusion

This study describes the design, synthesis and evaluation of fluorescent flipper probes with alkynes in their core. The insertion of one or two triple bonds is shown to advance their mechanosensitive ultrafast photophysics to a new level of sophistication and report selectively on thick membranes. Conventional flippers are twisted out of co-planarity by direct repulsion of sidechains that are in physical proximity across the twistable central bond. Core alkynylation removes this physical proximity between the push and the pull

domain of the planarizable push-pull probe. Rotation around the central alkynes becomes nearly barrier-less without strong preferences in the ground state, while planar conformers are preferred in the excited state because of PICT. This situation affords separate blue- and red-shifted absorption maxima for twisted and planar conformers. Selective excitation of twisted conformers results in viscosity-sensitive excited-state planarization followed by emission from the common red-shifted PICT state. This excited-state planarization competes with intersystem crossing into triplet states, which lower fluorescence intensity and lifetime.

Conventional flippers, introduced as planarizable push-pull probes, report on physical compression in equilibrium in the ground state with red-shifted excitation and also longer lifetimes because the FC state is equally planarized.^[41] Molecular rotors report on torsional motion off equilibrium in the excited state with lifetime changes but without shifted excitation maxima.^[40] The here introduced core expansion by alkynylation affords probes that merge these complementary characteristics on a new level where they can act like flippers, like rotors or a combination of both, depending on the environment.

In bulk solutions, comparably poor responsiveness to viscosity and temperature is more flipper- than rotor-like. In lipid bilayer membranes of common thickness, core-alkynylated flippers are poorly fluorescent even in ordered membranes because the pull domain of the elongated probes rotates more freely in the less ordered interleaflet space, while increasing deviations from uniform probe orientation are less important compared to positional disorder observed in disordered membranes. Core-alkynylated flippers light up in extra thick bilayers formed by lipids with tails of more than twenty carbons because hydrophobic matching of one leaflet with the elongated mechanophores increases planarization in the ground state, resulting in the red-shifted absorption and brighter fluorescence that are characteristic for flipper probes but not for molecular rotors. This result reveals hydrophobic matching with a single leaflet as sufficient and advantageous to fluorescently label lipid bilayer membranes according to their thickness. This access to responsive trackers of membranes of different thickness addresses a long-standing challenge in chemical biology and thus opens attractive perspectives in bioimaging.

Supporting Information

Experimental details, including references,^[53,61,70,71,89–103] preliminary results on the topic have been published in two PhD theses.^[104,105]

Acknowledgements

We thank the NMR, MS, ACCESS and Bioimaging platforms for services, and the University of Geneva, the National Centre of Competence in Research (NCCR) Molecular Systems Engineering (51NF40-205608), as well as the Swiss NSF for financial support (Excellence Grant

200020 204175; Swiss-ERC Advanced Grant TIMEUP, TMAG-2_209190; Grant 200020 184607). The computations were performed at University of Geneva using Baobab HPC service. Open Access funding provided by Université de Genève.

Conflict of Interest

The University of Geneva has licensed Flipper-TR[®] probes to Spirochrome for commercialization.

Data Availability Statement

The data that support the findings of this study are openly available in zenodo at <https://doi.org/10.5281/zenodo.11120575>.

Keywords: fluorescent probes · lipid bilayer membranes · planarizable push-pull probes · molecular rotors · mechanosensitive probes · hydrophobic matching · giant unilamellar vesicles

- [1] A. Vyšniauskas, M. Balaz, H. L. Anderson, M. K. Kuimova, *Phys. Chem. Chem. Phys.* **2015**, *17*, 7548–7554.
- [2] S. W. Thomas, G. D. Joly, T. M. Swager, *Chem. Rev.* **2007**, *107*, 1339–1386.
- [3] K. Sato, T. Muraoka, K. Kinbara, *Acc. Chem. Res.* **2021**, *54*, 3700–3709.
- [4] M. Štefko, M. D. Tzirakis, B. Breiten, M.-O. Ebert, O. Dumele, W. B. Schweizer, J.-P. Gisselbrecht, C. Boudon, M. T. Beels, I. Biaggio, F. Diederich, *Chem. Eur. J.* **2013**, *19*, 12693–12704.
- [5] W. A. Chalifoux, R. R. Tykwiński, *Chem. Rec.* **2006**, *6*, 169–182.
- [6] M. R. Bryce, *J. Mater. Chem. C* **2021**, *9*, 10524–10546.
- [7] N. P. Kamat, Z. Liao, L. E. Moses, J. Rawson, M. J. Therien, I. J. Dmochowski, D. A. Hammer, *Proc. Natl. Acad. Sci. USA* **2011**, *108*, 13984–13989.
- [8] J. E. Reeve, A. D. Corbett, I. Boczarow, W. Kaluza, W. Barford, H. Bayley, T. Wilson, H. L. Anderson, *Angew. Chem. Int. Ed.* **2013**, *52*, 9044–9048.
- [9] W. Hu, N. Zhu, W. Tang, D. Zhao, *Org. Lett.* **2008**, *10*, 2669–2672.
- [10] W. J. Mullin, P. Müller, A. J. Schaefer, E. Guzman, S. E. Wheeler, S. W. T. Iii, *J. Mater. Chem. C* **2022**, *10*, 11199–11210.
- [11] T. Muraoka, T. Shima, T. Hamada, M. Morita, M. Takagi, K. V. Tabata, H. Noji, K. Kinbara, *J. Am. Chem. Soc.* **2012**, *134*, 19788–19794.
- [12] K. Sato, R. Sasaki, R. Matsuda, M. Nakagawa, T. Ekimoto, T. Yamane, M. Ikeguchi, K. V. Tabata, H. Noji, K. Kinbara, *J. Am. Chem. Soc.* **2022**, *144*, 11802–11809.
- [13] T. Muraoka, K. Umetsu, K. V. Tabata, T. Hamada, H. Noji, T. Yamashita, K. Kinbara, *J. Am. Chem. Soc.* **2017**, *139*, 18016–18023.
- [14] N. Sakai, R. Bhosale, D. Emery, J. Mareda, S. Matile, *J. Am. Chem. Soc.* **2010**, *132*, 6923–6925.
- [15] S. A. McFarland, N. S. Finney, *J. Am. Chem. Soc.* **2002**, *124*, 1178–1179.

- [16] M. Levitus, K. Schmieder, H. Ricks, K. D. Shimizu, U. H. F. Bunz, M. A. Garcia-Garibay, *J. Am. Chem. Soc.* **2001**, *123*, 4259–4265.
- [17] A. N. Swinburne, M. J. Paterson, A. Beeby, J. W. Steed, *Chem. Eur. J.* **2010**, *16*, 2714–2718.
- [18] A. K. Pati, M. Mohapatra, P. Ghosh, S. J. Gharpure, A. K. Mishra, *J. Phys. Chem. A* **2013**, *117*, 6548–6560.
- [19] P. Moreno-García, M. Gulcur, D. Z. Manrique, T. Pope, W. Hong, V. Kaliginedi, C. Huang, A. S. Batsanov, M. R. Bryce, C. Lambert, T. Wandlowski, *J. Am. Chem. Soc.* **2013**, *135*, 12228–12240.
- [20] T. Luu, E. Elliott, A. D. Slepkov, S. Eisler, R. McDonald, F. A. Hegmann, R. R. Tykwiński, *Org. Lett.* **2005**, *7*, 51–54.
- [21] S. A. Sharber, S. W. Thomas, *Chem. Mater.* **2020**, *32*, 5785–5801.
- [22] W. Zhang, W. Sheng, C. Yu, Y. Wei, H. Wang, E. Hao, L. Jiao, *Chem. Commun.* **2017**, *53*, 5318–5321.
- [23] J. D. Kimball, S. Raut, L. P. Jameson, N. W. Smith, Z. Gryczynski, S. V. Dzyuba, *RSC Adv.* **2015**, *5*, 19508–19511.
- [24] S. L. Raut, J. D. Kimball, R. Fudala, I. Bora, R. Chib, H. Jafari, M. K. Castillo, N. W. Smith, I. Gryczynski, S. V. Dzyuba, Z. Gryczynski, *Phys. Chem. Chem. Phys.* **2016**, *18*, 4535–4540.
- [25] M. Rickhaus, A. Vargas Jentzsch, L. Tejerina, I. Grübner, M. Jirasek, T. D. W. Claridge, H. L. Anderson, *J. Am. Chem. Soc.* **2017**, *139*, 16502–16505.
- [26] H. Doan, S. L. Raut, D. Yale, M. Balaz, S. V. Dzyuba, Z. Gryczynski, *Chem. Commun.* **2016**, *52*, 9510–9513.
- [27] M. K. Kuimova, M. Balaz, H. L. Anderson, P. R. Ogilby, *J. Am. Chem. Soc.* **2009**, *131*, 7948–7949.
- [28] I. Fureraj, D. S. Budkina, E. Vauthey, *Phys. Chem. Chem. Phys.* **2022**, *24*, 25979–25989.
- [29] T. Luu, E. Elliott, A. D. Slepkov, S. Eisler, R. McDonald, F. A. Hegmann, R. R. Tykwiński, *Org. Lett.* **2005**, *7*, 51–54.
- [30] J. Li, Y. Zhang, H. Zhang, X. Xuan, M. Xie, S. Xia, G. Qu, H. Guo, *Anal. Chem.* **2016**, *88*, 5554–5560.
- [31] C. Wang, L.-O. Pálsson, A. S. Batsanov, M. R. Bryce, *J. Am. Chem. Soc.* **2006**, *128*, 3789–3799.
- [32] M. Pérez-Pérez, I. López-Duarte, A. Vyšniauskas, N. J. Brooks, M. K. Kuimova, *Chem. Sci.* **2020**, *12*, 2604–2613.
- [33] I. López-Duarte, P. Chairatana, Y. Wu, J. Pérez-Moreno, P. M. Bennett, J. E. Reeve, I. Boczarow, W. Kaluza, N. A. Hosny, S. D. Stranks, R. J. Nicholas, K. Clays, M. K. Kuimova, H. L. Anderson, *Org. Biomol. Chem.* **2015**, *13*, 3792–3802.
- [34] L.-O. Pálsson, C. Wang, A. S. Batsanov, S. M. King, A. Beeby, A. P. Monkman, M. R. Bryce, *Chem. Eur. J.* **2010**, *16*, 1470–1479.
- [35] H. Nakayama, S. Kimura, *J. Phys. Chem. A* **2011**, *115*, 8960–8968.
- [36] E. González-Rodríguez, B. Guzmán-Juárez, M. Miranda-Olvera, M. del P Carreón-Castro, M. Maldonado-Domínguez, R. Arcos-Ramos, N. Farfán, R. Santillan, *Spectrochim. Acta. Mol. Biomol. Spectrosc.* **2022**, *267*, 120520.
- [37] S. Xia, M. Fang, J. Wang, J. Bi, W. Mazi, Y. Zhang, R. L. Luck, H. Liu, *Sens. Actuators B* **2019**, *294*, 1–13.
- [38] Y. Rout, C. Montanari, E. Pasciucco, R. Misra, B. Carlotti, *J. Am. Chem. Soc.* **2021**, *143*, 9933–9943.
- [39] A. Tigleros, A. Ortiz, B. Insuasty, *Dyes Pigm.* **2014**, *111*, 45–51.
- [40] M. Paez-Perez, M. Kuimova, *Angew. Chem. Int. Ed.* **2023**, *62*, e202311233.
- [41] X.-X. Chen, F. Bayard, N. Gonzalez-Sanchis, K. K. P. Pamungkas, N. Sakai, S. Matile, *Angew. Chem. Int. Ed.* **2023**, *62*, e202217868.
- [42] E. Pandzic, R. Whan, A. Macmillan, in *Membr. Lipids Methods Protoc.* (Ed.: C. G. Cranfield), Springer US, New York, NY, **2022**, pp. 257–283.
- [43] Z.-H. Wang, C. Combs, W. Zhao, H. Xu, *STAR Protoc.* **2024**, *5*, 102959.
- [44] B. Baumeister, S. Matile, *Chem. Eur. J.* **2000**, *6*, 1739–1749.
- [45] J.-Y. Winum, S. Matile, *J. Am. Chem. Soc.* **1999**, *121*, 7961–7962.
- [46] A. Fin, A. Vargas Jentzsch, N. Sakai, S. Matile, *Angew. Chem. Int. Ed.* **2012**, *51*, 12736–12739.
- [47] L. Assies, V. Mercier, J. López-Andarias, A. Roux, N. Sakai, S. Matile, *ChemBioChem* **2022**, *23*, e202200192.
- [48] F. Piazzolla, V. Mercier, L. Assies, N. Sakai, A. Roux, S. Matile, *Angew. Chem. Int. Ed.* **2021**, *60*, 12258–12263.
- [49] J. García-Calvo, J. López-Andarias, J. Maillard, V. Mercier, C. Roffay, A. Roux, A. Fürstenberg, N. Sakai, S. Matile, *Chem. Sci.* **2022**, *13*, 2086–2093.
- [50] J. López-Andarias, K. Eblighatian, Q. T. L. Pasquer, L. Assies, N. Sakai, S. Hoogendoorn, S. Matile, *Angew. Chem. Int. Ed.* **2022**, *61*, e202113163.
- [51] J. López-Andarias, K. Straková, R. Martinent, N. Jiménez-Rojo, H. Riezman, N. Sakai, S. Matile, *JACS Au* **2021**, *1*, 221–232.
- [52] J. García-Calvo, J. López-Andarias, N. Sakai, S. Matile, *Chem. Commun.* **2021**, *57*, 3913–3916.
- [53] J. García-Calvo, J. López-Andarias, N. Sakai, S. Matile, *Helv. Chim. Acta* **2022**, *105*, e202100238.
- [54] N. Sakai, L. Assies, S. Matile, *Helv. Chim. Acta* **2022**, *105*, e202200052.
- [55] A. S. Klymchenko, *Acc. Chem. Res.* **2017**, *50*, 366–375.
- [56] A. S. Klymchenko, *Acc. Chem. Res.* **2023**, *56*, 1–12.
- [57] P. Liu, E. W. Miller, *Acc. Chem. Res.* **2020**, *53*, 11–19.
- [58] T. Baumgart, G. Hunt, E. R. Farkas, W. W. Webb, G. W. Feigenson, *Biochim. Biophys. Acta* **2007**, *1768*, 2182–2194.
- [59] E. Sezgin, T. Sadowski, K. Simons, *Langmuir* **2014**, *30*, 8160–8166.
- [60] B. Ghebremariam, V. Sidorov, S. Matile, *Tetrahedron Lett.* **1999**, *40*, 1445–1448.
- [61] M. Macchione, M. Tsemperouli, A. Goujon, A. R. Mallia, N. Sakai, K. Sugihara, S. Matile, *Helv. Chim. Acta* **2018**, *101*, e1800014.
- [62] P. Müller, J. Nikolaus, S. Schiller, A. Herrmann, K. Möllnitz, S. Czapla, P. Wessig, *Angew. Chem. Int. Ed.* **2009**, *48*, 4433–4435.
- [63] T. Chen, A. Ghosh, J. Enderlein, *Nano Lett.* **2023**, *23*, 2421–2426.
- [64] M. R. R. de Planque, J. A. Killian, *Mol. Membr. Biol.* **2003**, *20*, 271–284.
- [65] J. A. Killian, G. von Heijne, *Trends Biochem. Sci.* **2000**, *25*, 429–434.
- [66] R. Prasad, A. Sliwa-Gonzalez, Y. Barral, *Sci. Adv.* **2020**, *6*, eaba5130.
- [67] S. Rodriguez-Gallardo, K. Kurokawa, S. Sabido-Bozo, A. Cortes-Gomez, A. Ikeda, V. Zoni, A. Aguilera-Romero, A. M. Perez-Linero, S. Lopez, M. Waga, M. Araki, M. Nakano, H. Riezman, K. Funato, S. Vanni, A. Nakano, M. Muñiz, *Sci. Adv.* **2020**, *6*, eaba8237.
- [68] J. H. Lorent, K. R. Levental, L. Ganesan, G. Rivera-Longsworth, E. Sezgin, M. Doktorova, E. Lyman, I. Levental, *Nat. Chem. Biol.* **2020**, *16*, 644–652.
- [69] N. Sakai, N. Majumdar, S. Matile, *J. Am. Chem. Soc.* **1999**, *121*, 4294–4295.
- [70] W. Yin, C. He, M. Chen, H. Zhang, A. Lei, *Org. Lett.* **2009**, *11*, 709–712.
- [71] A. Elangovan, Y.-H. Wang, T.-I. Ho, *Org. Lett.* **2003**, *5*, 1841–1844.
- [72] M. L. Horng, J. A. Gardecki, A. Papazyan, M. Maroncelli, *J. Phys. Chem.* **1995**, *99*, 17311–17337.
- [73] M. R. Wasielewski, D. G. Johnson, W. A. Svec, K. M. Kersey, D. W. Minsek, *J. Am. Chem. Soc.* **1988**, *110*, 7219–7221.

- [74] B. F. Habenicht, O. V. Prezhdo, *J. Am. Chem. Soc.* **2012**, *134*, 15648–15651.
- [75] F. Franco de Carvalho, C. A. Pignedoli, I. Tavernelli, *J. Phys. Chem. C* **2017**, *121*, 10140–10152.
- [76] K. Nagarajan, A. R. Mallia, K. Muraleedharan, M. Hariharan, *Chem. Sci.* **2017**, *8*, 1776–1782.
- [77] R. Letrun, B. Lang, O. Yushchenko, R. Wilcken, D. Svechkarev, D. Kolodieznyi, E. Riedle, E. Vauthey, *Phys. Chem. Chem. Phys.* **2018**, *20*, 30219–30230.
- [78] Y. Wu, M. Stefl, A. Olzyńska, M. Hof, G. Yahioglu, P. Yip, D. R. Casey, O. Ces, J. Humpolíčková, M. K. Kuimova, *Phys. Chem. Chem. Phys.* **2013**, *15*, 14986–93.
- [79] V. Adrien, G. Rayan, K. Astafyeva, I. Broutin, M. Picard, P. Fuchs, W. Urbach, N. Taulier, *Biophys. Chem.* **2022**, *281*, 106732.
- [80] T. Förster, G. Hoffmann, *Z. für Phys. Chem.* **1971**, *75*, 63–76.
- [81] G. Licari, K. Strakova, S. Matile, E. Tajkhorshid, *Chem. Sci.* **2020**, *11*, 5637–5649.
- [82] Y. Wu, M. Štefl, A. Olzyńska, M. Hof, G. Yahioglu, P. Yip, D. R. Casey, O. Ces, J. Humpolíčková, M. K. Kuimova, *Phys. Chem. Chem. Phys.* **2013**, *15*, 14986–14993.
- [83] F. Bayard, X.-X. Chen, J. M. García-Arcos, A. Roux, N. Sakai, S. Matile, *ChemistryEurope* **2023**, *1*, e202300041.
- [84] S. Ranjit, L. Malacrida, D. M. Jameson, E. Gratton, *Nat. Protoc.* **2018**, *13*, 1979–2004.
- [85] W. Grudzinski, J. Sagan, R. Welc, R. Luchowski, W. I. Gruszecki, *Sci. Rep.* **2016**, *6*, 32780.
- [86] J. M. Holopainen, A. J. Metso, J.-P. Mattila, A. Jutila, P. K. J. Kinnunen, *Biophys. J.* **2004**, *86*, 1510–1520.
- [87] T. Róg, M. Pasenkiewicz-Gierula, *Biophys. J.* **2006**, *91*, 3756–3767.
- [88] I. Bera, J. B. Klauda, *J. Phys. Chem. B* **2017**, *121*, 5197–5208.
- [89] X.-X. Chen, R. M. Gomila, J. M. García-Arcos, M. Vonesch, N. Gonzalez-Sanchis, A. Roux, A. Frontera, N. Sakai, S. Matile, *JACS Au* **2023**, *3*, 2557–2565.
- [90] M. Dal Molin, Q. Verolet, A. Colom, R. Letrun, E. Derivery, M. Gonzalez-Gaitan, E. Vauthey, A. Roux, N. Sakai, S. Matile, *J. Am. Chem. Soc.* **2015**, *137*, 568–571.
- [91] J. Grünwald, Y. Jin, J. Vance, J. Read, X. Wang, Y. Wan, H. Zhou, W. Ou, H. E. Klock, E. C. Peters, T. Uno, A. Brock, B. H. Geierstanger, *Bioconjugate Chem.* **2017**, *28*, 1906–1915.
- [92] J. Sinha, R. Sahoo, A. Kumar, *Macromolecules* **2009**, *42*, 2015–2022.
- [93] M. J. Frisch, G. W. Trucks, H. B. Schlegel, G. E. Scuseria, M. A. Robb, J. R. Cheeseman, G. Scalmani, V. Barone, G. A. Petersson, H. Nakatsuji, X. Li, M. Caricato, A. V. Marenich, J. Bloino, B. G. Janesko, R. Gomperts, B. Mennucci, H. P. Hratchian, J. V. Ortiz, A. F. Izmaylov, J. L. Sonnenberg, Williams, F. Ding, F. Lipparini, F. Egidi, J. Goings, B. Peng, A. Petrone, T. Henderson, D. Ranasinghe, V. G. Zakrzewski, J. Gao, N. Rega, G. Zheng, W. Liang, M. Hada, M. Ehara, K. Toyota, R. Fukuda, J. Hasegawa, M. Ishida, T. Nakajima, Y. Honda, O. Kitao, H. Nakai, T. Vreven, K. Throssell, J. A. Montgomery Jr., J. E. Peralta, F. Ogliaro, M. J. Bearpark, J. J. Heyd, E. N. Brothers, K. N. Kudin, V. N. Staroverov, T. A. Keith, R. Kobayashi, J. Normand, K. Raghavachari, A. P. Rendell, J. C. Burant, S. S. Iyengar, J. Tomasi, M. Cossi, J. M. Millam, M. Klene, C. Adamo, R. Cammi, J. W. Ochterski, R. L. Martin, K. Morokuma, O. Farkas, J. B. Foresman, D. J. Fox, *Gaussian 16 Rev. C.01*, Wallingford, CT, **2016**.
- [94] T. Yanai, D. P. Tew, N. C. Handy, *Chem. Phys. Lett.* **2004**, *393*, 51–57.
- [95] J. D. Thompson, P. Winget, D. G. Truhlar, *PhysChemComm* **2001**, *4*, 72–77.
- [96] J. Deng, A. T. B. Gilbert, P. M. W. Gill, *J. Chem. Theory Comput.* **2015**, *11*, 1639–1644.
- [97] A. Astar, G. Licari, F. Zinna, E. Brun, T. Kumpulainen, E. Tajkhorshid, J. Lacour, E. Vauthey, *Chem. Sci.* **2019**, *10*, 10629–10639.
- [98] J. S. Beckwith, A. Astar, E. Vauthey, *Phys. Chem. Chem. Phys.* **2021**, *24*, 568–577.
- [99] B. Lang, S. Mosquera-Vázquez, D. Lovy, P. Sherin, V. Markovic, E. Vauthey, *Rev. Sci. Instrum.* **2013**, *84*, 073107.
- [100] J. Maillard, K. Klehs, C. Rumble, E. Vauthey, M. Heilemann, A. Fürstenberg, *Chem. Sci.* **2021**, *12*, 1352–1362.
- [101] M. Wojdyr, *J. Appl. Crystallogr.* **2010**, *43*, 1126–1128.
- [102] R. Koynova, M. Caffrey, *Biochim. Biophys. Acta BBA- - Rev. Biomembr.* **1998**, *1376*, 91–145.
- [103] R. B. Lira, J. Steinkühler, R. L. Knorr, R. Dimova, K. A. Riske, *Sci. Rep.* **2016**, *6*, 25254.
- [104] I. Fureraj, Dynamics of Primary Relaxation Phenomena upon Photoexcitation of Conjugated Molecules in Liquids, Université de Genève, **2023**.
- [105] L. Assies, Fluorescent Membrane Tension Reporters: Core Alkynylation and Intracellular Tracking Rules for Specific Targeting, Université de Genève, **2022**.

Manuscript received: April 1, 2024

Accepted manuscript online: May 17, 2024

Version of record online: June 26, 2024